doi:10.1038/nature12240

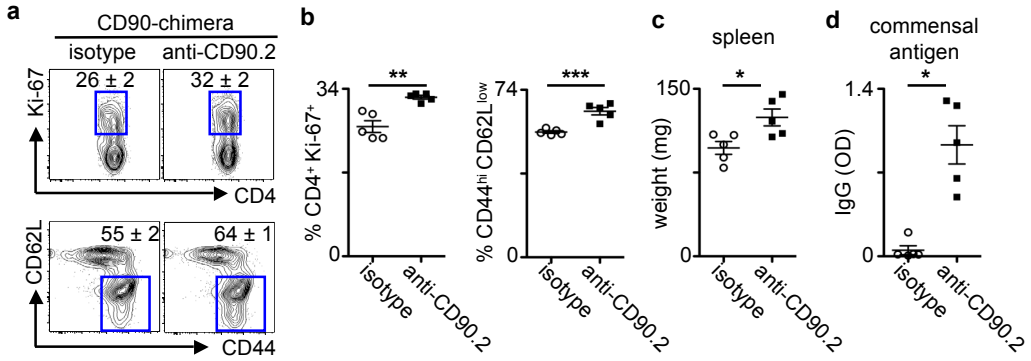

Figure S1. Experimental depletion of innate lymphoid cells results in dysregulated adaptive immune cell responses to commensal bacteria.
a-**d**, Defined age- and sex-matched CD90-disparate mouse chimeras were continuously treated with anti-CD90.2 monoclonal antibody for 14 days and examined for the frequency of splenic Ki-67^{+} CD4^{+} T cells (top) and CD44^{high} CD62L^{low} CD4^{+} T cells (bottom) (**a**), quantified frequencies of splenic Ki-67^{+} CD4^{+} T cells (left) and CD44^{high} CD62L^{low} CD4^{+} T cells (right) (**b**), spleen weight (**c**) and relative optical density (OD) values of serum IgG specific to commensal bacteria (**d**). Flow cytometry plots are gated on live CD4^{+} CD3^{+} T cells (**a**). Data are representative of 2 independent experiments containing 3-5 mice per group. Results are shown as the means +/- s.e.m. * $p < 0.05$, ** $p < 0.01$, *** $p < 0.001$ (two-tailed students *t*-test).

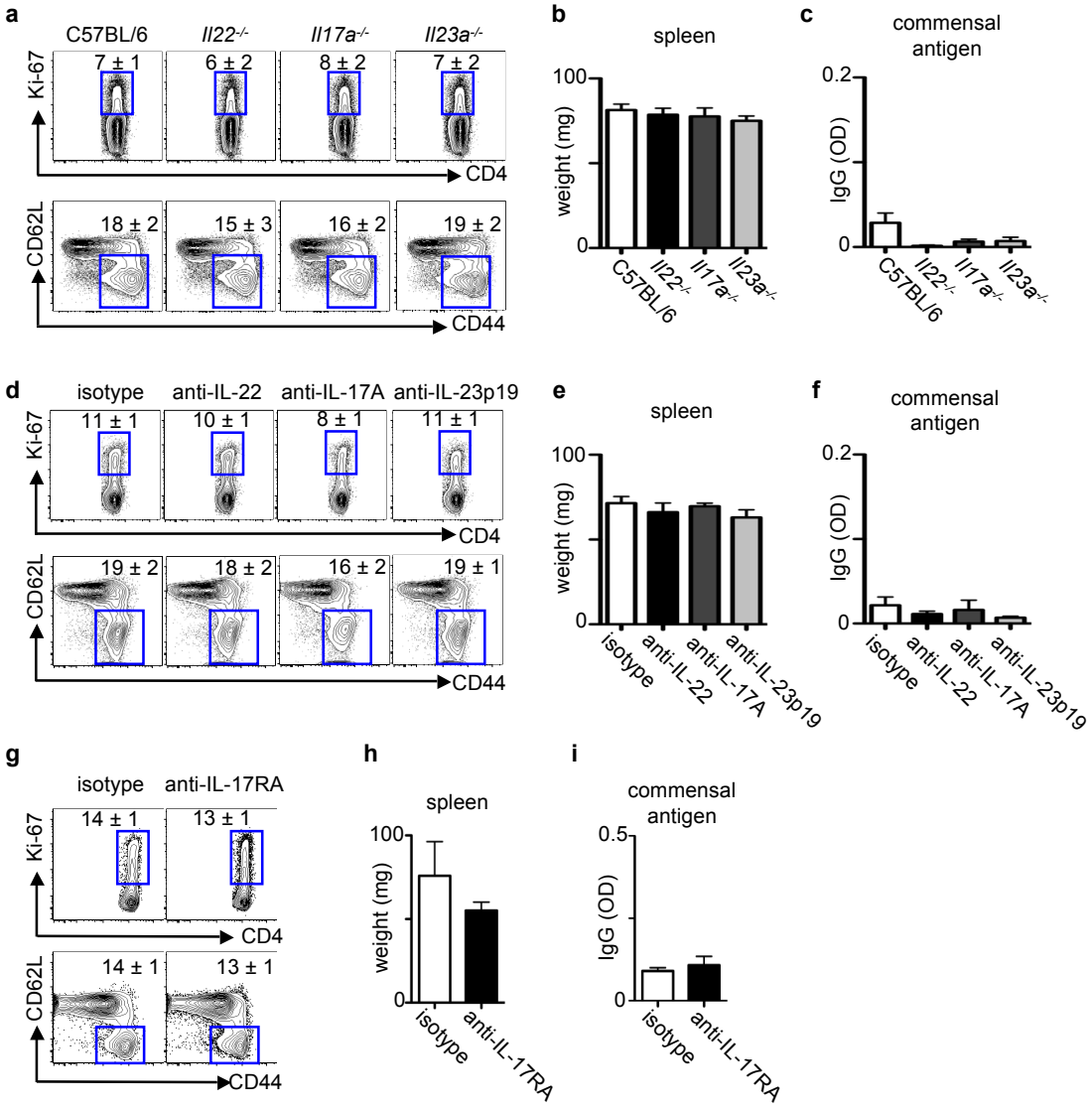

Figure S2. Genetic deletion or experimental blockade of IL-22, IL-17A, IL-23p19 or IL-17RA does not result in dysregulated adaptive immune cell responses to commensal bacteria. **a**-**c**, Defined age- and sex-matched control and cytokine-deficient mice, or C57BL/6 mice that were continuously treated with monoclonal antibodies for 14 days, were examined for the frequency of splenic Ki-67^{+} CD4^{+} T cells (top) and CD44^{high} CD62L^{low} CD4^{+} T cells (bottom) (**a**,**d**,**g**), spleen weight (**b**,**e**,**h**) and relative optical density (OD) values of serum IgG specific to commensal bacteria (**c**,**f**,**i**). Flow cytometry plots are gated on live CD4^{+} CD3^{+} T cells (**a**,**d**,**g**). Data are representative of 2 independent experiments containing 3-5 mice per group. Results are shown as the means +/- s.e.m.

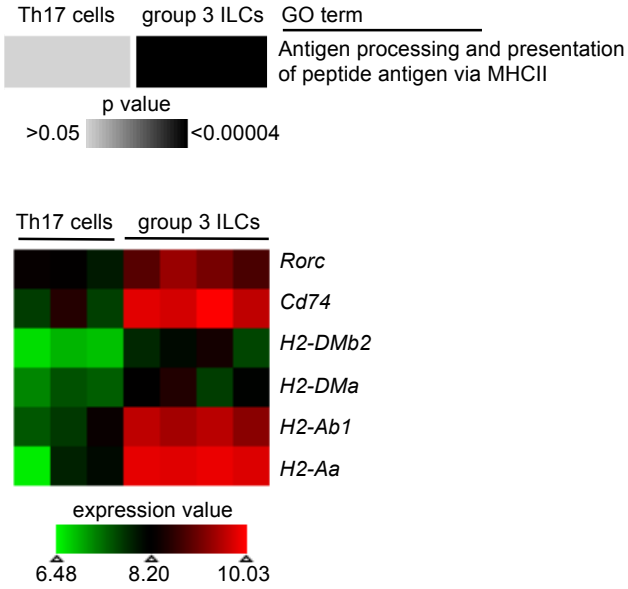

Figure S3. RORγt⁺ group 3 innate lymphoid cells are enriched in MHCII-associated gene transcripts as compared to RORγt⁺ T helper 17 cells. DAVID pathway analysis of GO terms enriched in the transcriptional profiles of *in vitro* differentiated Th17 cells and group 3 RORγt⁺ ILCs (top) and heat map of selected lymphoid-associated and MHCII-associated gene transcripts (bottom).

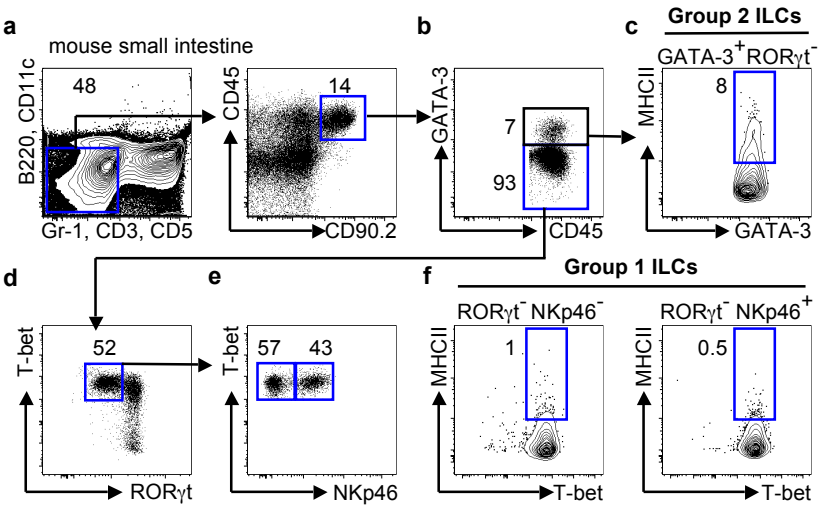

Figure S4. Expression of MHCII on group 1 and group 2 ILCs. **a**-**f**, Gating strategy to identify total Lineage$^-$ ILCs (**a**), group 2 ILCs (**b**) and group 1 ILCs (**d**,**e**). Expression of MHCII in GATA-3$^+$ group 2 ILCs (**c**) and T-bet$^+$ RORγt$^-$ group 1 ILCs subsets (**e**,**f**) in the small intestine of naive mice. Data are representative of 2 independent experiments containing 2-3 mice per group.

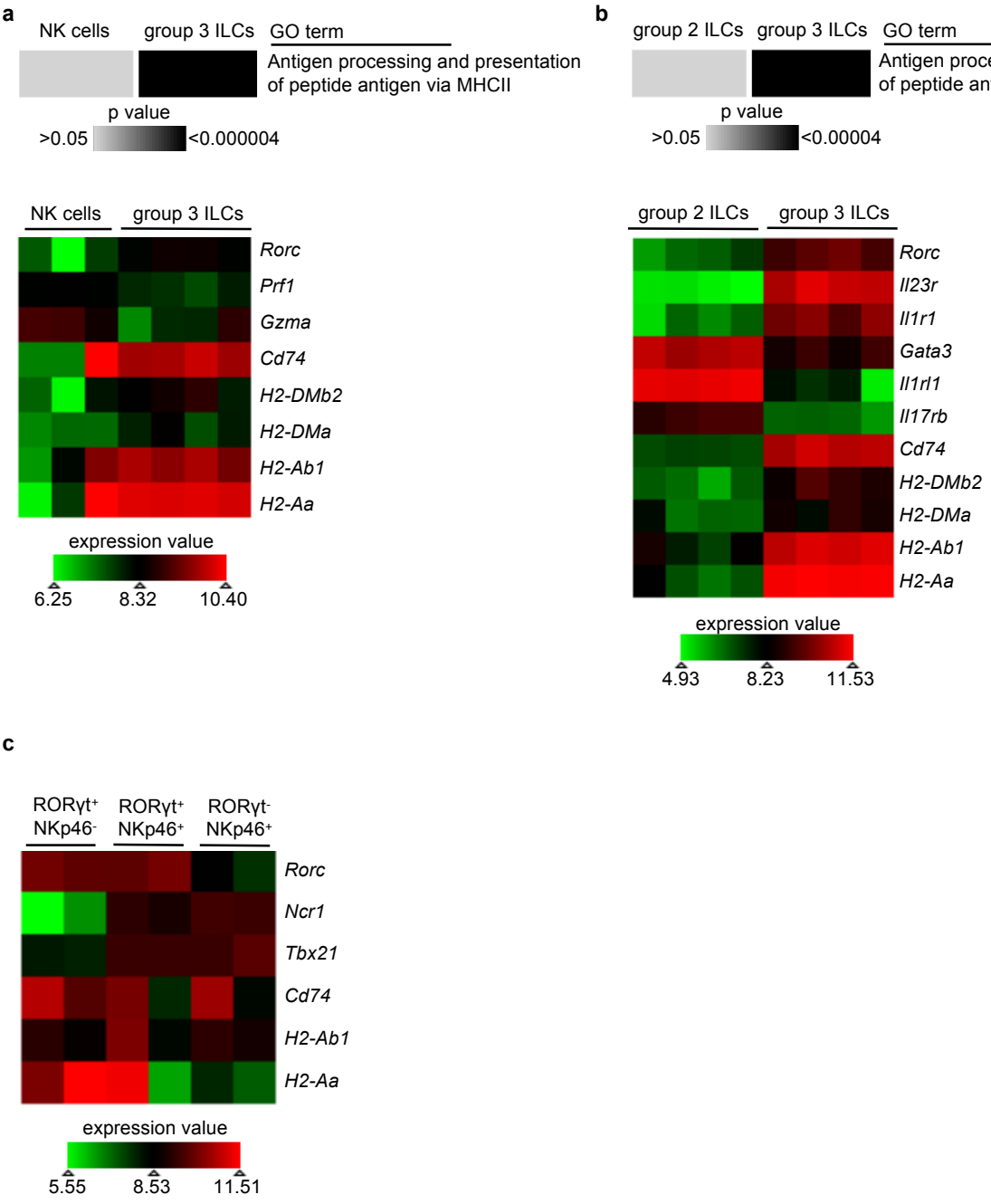

Figure S5. T-bet^{-} NKp46^{-} RORγt^{+} ILCs are enriched in MHCII-associated gene transcripts as compared group 1, group 2 and T-bet^{+} NKp46$^{+/-}$ RORγt^{+} ILCs. **a**, DAVID pathway analysis of GO terms enriched in the transcriptional profiles of splenic NK cells and group 3 RORγt^{+} ILCs (top) and heat map of selected lymphoid-associated and MHCII-associated gene transcripts (bottom). **b**, DAVID pathway analysis of GO terms enriched in the transcriptional profiles of group 2 ILCs and group 3 RORγt^{+} ILCs (top) and heat map of selected lymphoid-associated and MHCII-associated gene transcripts (bottom). **c**, Heat map of selected lymphoid-associated and MHCII-associated gene transcripts in the transcriptional profiles of ILC subgroups distinguished by RORγt and NKp46.

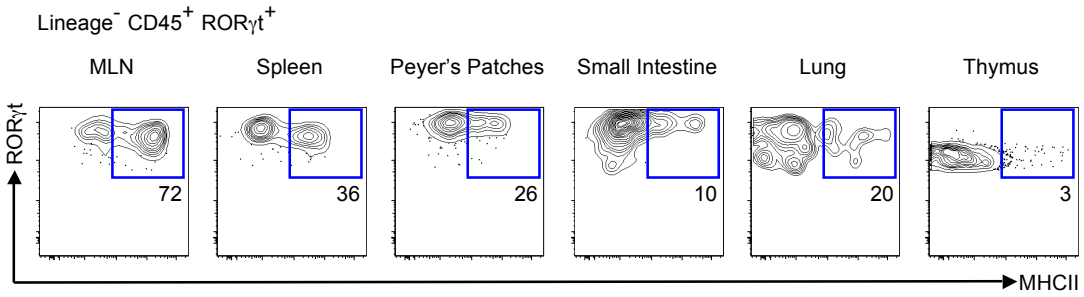

Figure S6. MHCII expression is enriched in RORγt⁺ ILCs in lymphoid tissues. Lineage⁻ CD45⁺ RORγt⁺ ILCs were examined for expression of MHCII in various lymphoid and mucosal tissues. Data are representative of 2 independent experiments containing 2-3 mice per group.

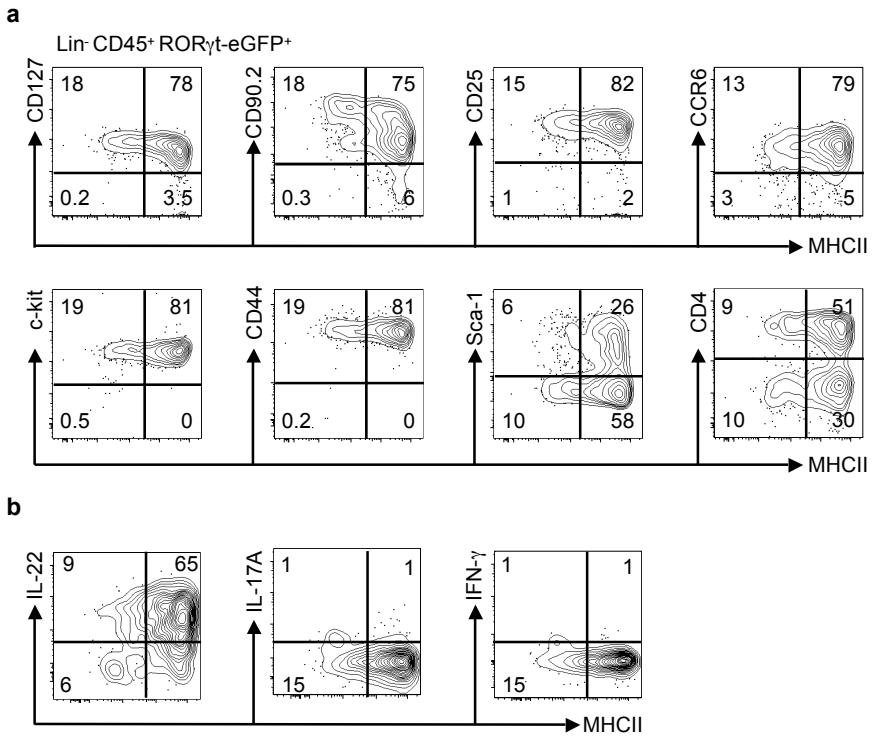

Figure S7. Phenotypic analysis of MHCII⁺ RORγt⁺ ILCs. mLN cells from RORγt-eGFP mice were gated as Lineage⁻ CD45⁺ RORγt-eGFP⁺ and expression of defined surface makers on MHCII expressing ILCs quantified (**a**). Expression of IL-22, IL-17A and IFN-γ by MHCII⁺ ILCs following 4 hours *ex vivo* restimulation with IL-23 (**b**). Data are representative of 2 independent experiments containing 2-3 mice per group.

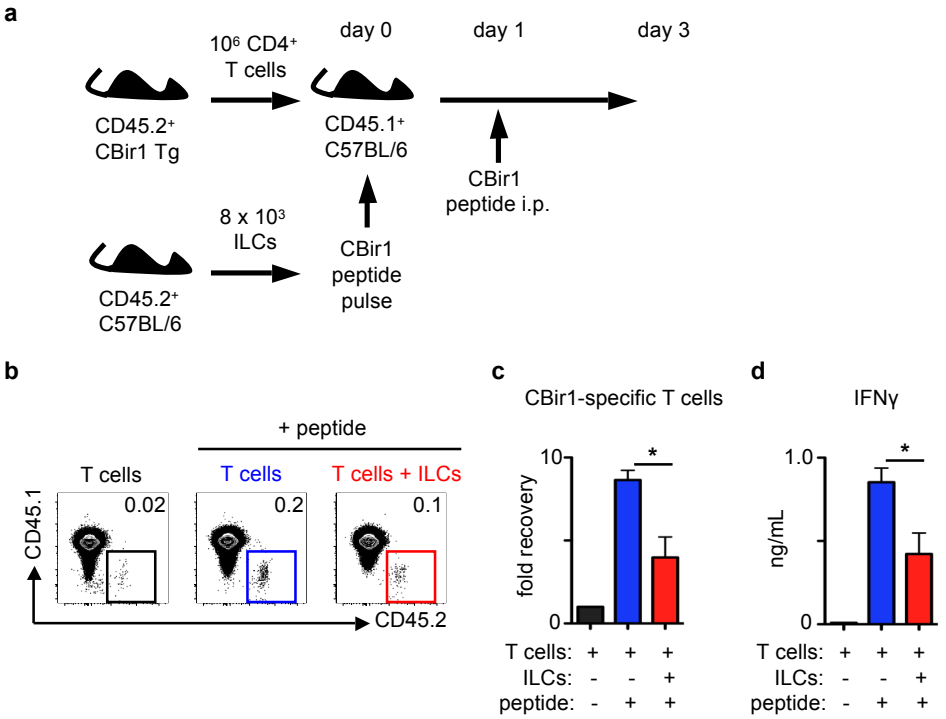

Figure S8. ILC-T cell interactions limit the magnitude of T cell responses to commensal bacteria-specific antigens. a, Sort-purified CBir1 TCR transgenic CD4⁺ T cells were transferred into congenically marked hosts with or without co-transfer of sort-purified and CBir1 peptide pulsed ILCs. 24 hours later mice were systemically challenged with CBir1 peptide. **b-d** Three days following peptide challenge, recovery of total transgenic T cells from the spleen was quantified (**b,c**) and peptide-specific IFN-γ production was quantified following *in vitro* restimulation (**d**). Data are representative of 2 independent experiments containing 2-3 mice per group. Results are shown as the means +/- s.e.m. * $p < 0.05$ (two-tailed students *t*-test).

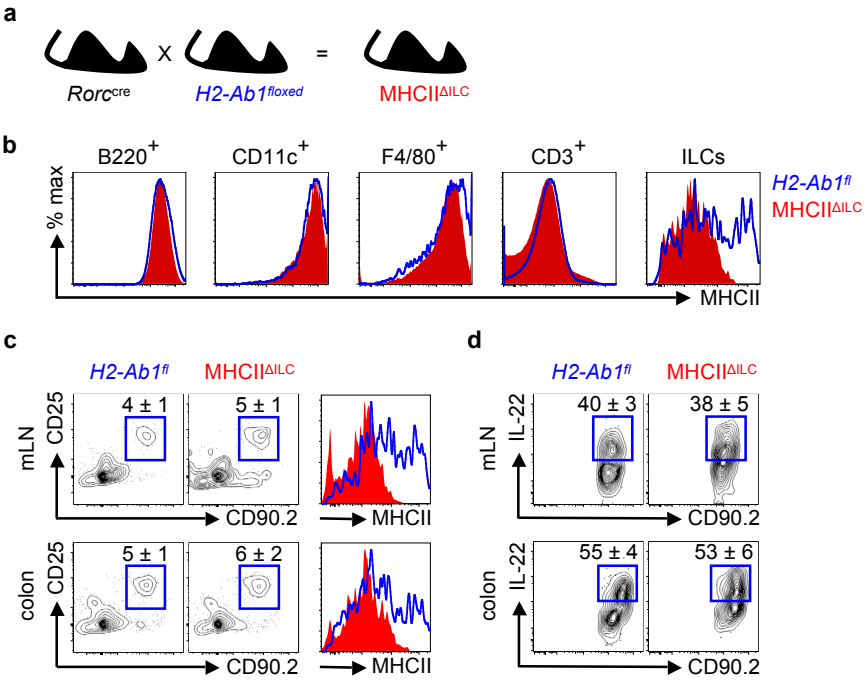

Figure S9. Deletion of RORγt⁺ innate lymphoid cell-intrinsic MHCII does not alter ILC frequency or cytokine production.
a, **b**, Mouse strains crossed to generate MHCII$^{\Delta ILC}$ mice (**a**) and expression of MHCII in gated populations in the mLN of control *H2-Ab1^{floxed}* mice (blue) or MHCII$^{\Delta ILC}$ mice (red) (**b**). **c, d,** *H2-Ab1^{floxed}* mice or MHCII$^{\Delta ILC}$ mice were examined for the frequency of lineage$^-$ CD90.2$^+$ CD25$^+$ ILCs (**c**) and IL-22$^+$ ILCs (**d**). Flow cytometry plots are gated on Lineage$^-$ CD90.2$^+$ CD25$^+$ ILCs **(c,d).** Data are representative of 2 independent experiments containing 3-5 mice per group. Results are shown as the means +/- s.e.m.

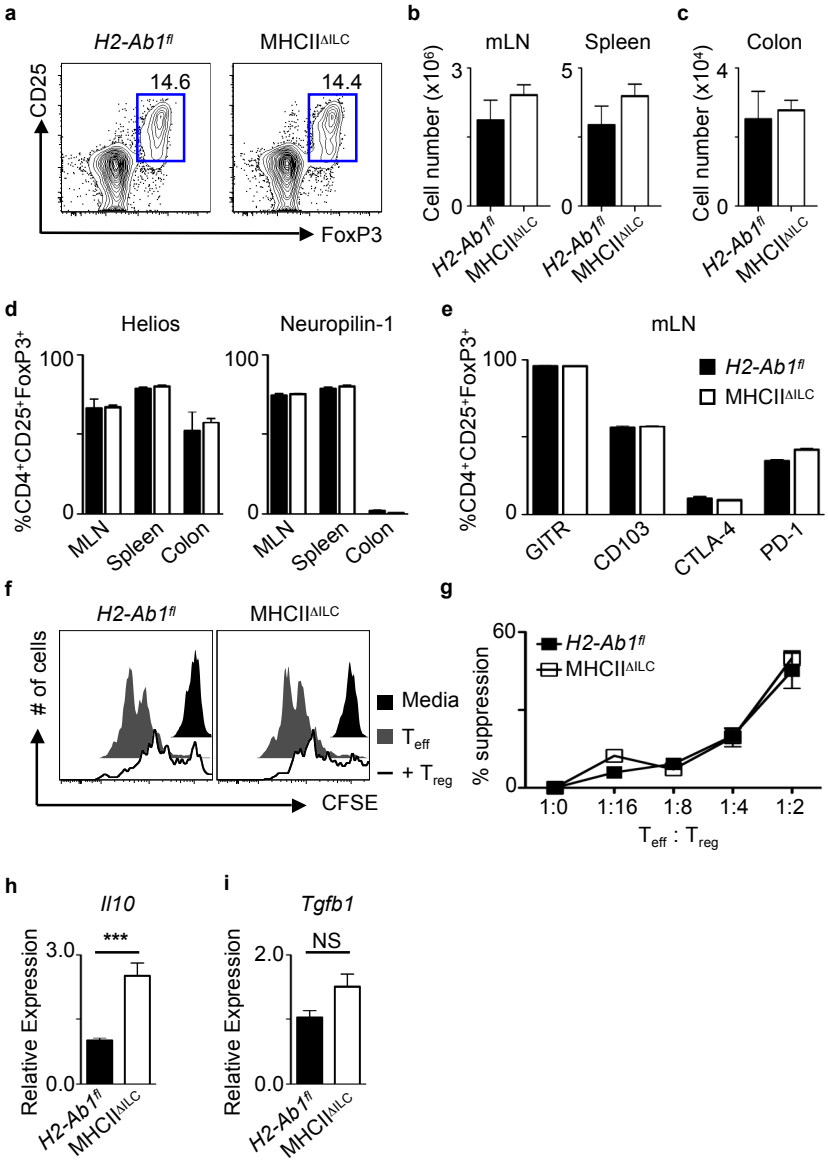

Figure S10. Deletion of RORγt⁺ innate lymphoid cell-intrinsic MHCII does not alter the frequency, phenotype or function of CD4⁺ CD25⁺ FoxP3⁺ regulatory T cells. **a**-**c**, *H2-Ab1*^{floxed} mice or MHCII$^{\Delta ILC}$ mice were examined for the frequency (**a**) and total cell number of CD4⁺ CD25⁺ FoxP3⁺ T cells in the mLN and spleen (**b**) and colon (**c**). Flow cytometry plots are gated on live CD3⁺ CD4⁺ T cells in the mLN (**a**). **d**,**e** Expression of Helios and Neuropilin-1 in various tissues (**d**) and GITR, CD103, CTLA-4 and PD1 in the mLN (**e**) were quantified on CD4⁺ CD25⁺ FoxP3⁺ T cells. **f**,**g,** Sort-purified CD4⁺ CD25⁺ CD45RB^{lo} regulatory T cells (>98% FoxP3⁺) were added to sort-purified CFSE-labeled effector T cells (CD4⁺, CD25^{-}, CD45RB^{hi}) in the presence of purified CD11c⁺ DCs and soluble anti-CD3 (**f**) and CFSE dilution was quantified (**g**). **h**,**i** *H2-Ab1*^{floxed} mice or MHCII$^{\Delta ILC}$ mice were examined for expression levels of *Il10* (**h**) or *Tgfb* (**i**) in the colon. NS, not significant. Data are representative of 2 independent experiments containing 1-3 mice per group or 2-4 *in vitro* replicates. Results are shown as the means +/- s.e.m. *** $p < 0.001$ (two-tailed students *t*-test).

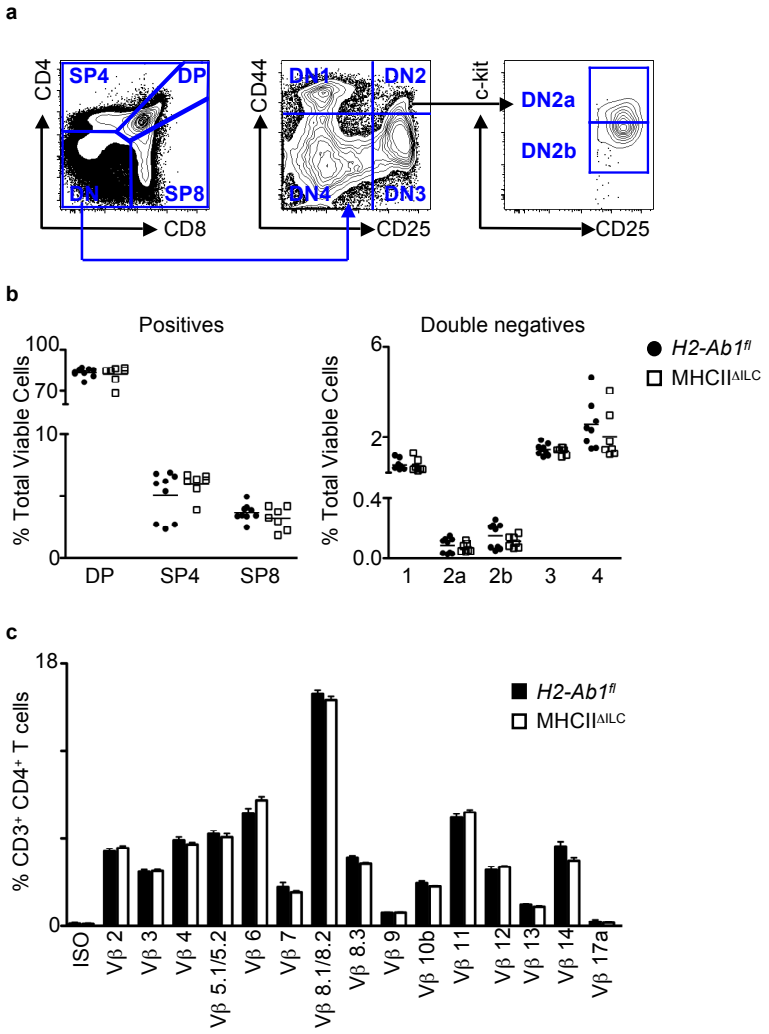

Figure S11. Thymic selection is not affected by the deletion of ILC-intrinsic MHCII. Defined age- and sex-matched mouse strains were examined for thymocyte maturation and peripheral TCR usage. **a**-**c**, Gating strategy to identify stages of thymocyte development (**a**). *H2-Ab1*^{floxed} mice or MHCII$^{\Delta ILC}$ mice were examined for the frequency of thymocytes at different stages of development (**b**). Expression of TCR vβ chains in splenic CD4^{+} T cells (**c**). Data are representative of 2 independent experiments containing 2-3 mice per group. Results are shown as the means +/- s.e.m.

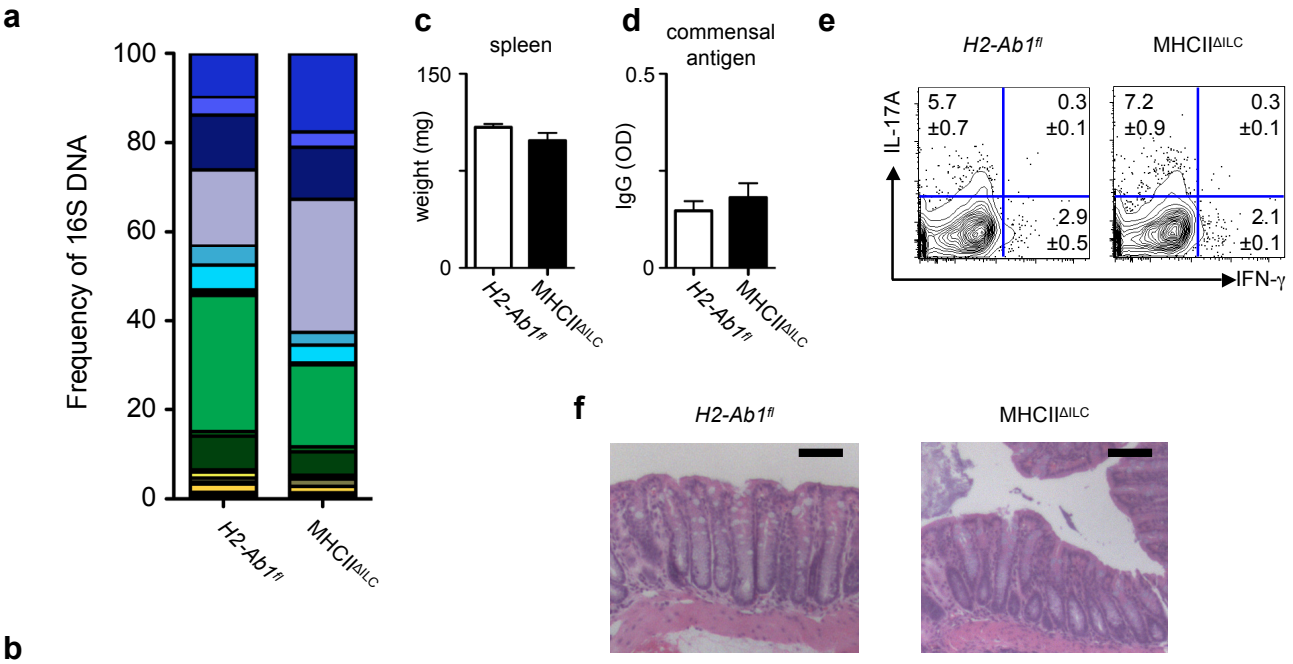

b

Phylum	Class	Order	Family
Bacteroidetes	Bacteroidia	Bacteroidales	Bacteroidaceae
			Other
			Porphyromoadaceae
			Prevotellaceae
			Rikenellaceae
	Other	Other	Other
	Sphingobacteria	Sphingobacteriales	Flammeovirgaceae
Deferribacteres	Deferribacteres	Defferibacterales	Deferribacteraceae
Firmicutes	Bacilli	Lactobacillales	Lactobacillaceae
	Clostridia	Clostridiales	Lachnospiraceae
			Other
			Ruminococcaceae
Other	Other	Other	Other
Proteobacteria	Alphaproteobacteria	Other	Other
	Betaproteobacteria	Burkholderiales	Sutterellaceae
	Epsilonproteobacteria	Campylobacterales	Helicobacteraceae
	Other	Other	Other
TM7	TM7	TM7	TM7
Tenericutes	Mollicutes	Anaeroplamatales	Anaeroplasmataceae

Figure S12. Intestinal inflammation is not the result of dysbiosis in the absence of RORγt⁺ innate lymphoid cell-intrinsic MHCII. The composition of the intestinal microbiota was examined in defined age- and sex-matched co-housed mouse strains. **a-f** Relative abundance of family-level commensal bacteria obtained from 16S pyrosequencing of the luminal colonic contents of age-matched littermate *H2-Ab1*^{floxed} mice and MHCII$^{\Delta ILC}$ mice (**a**) and list of detected bacterial families (**b**). Transfer of cecal contents from littermate *H2-Ab1*^{floxed} mice and MHCII$^{\Delta ILC}$ mice to germ free mice via oral gavage and assessment of splenic weight (**c**), commensal bacteria antigen-specific serum IgG (**d**), CD4⁺ T cell cytokine production (**e**) and colon histology (**f**) 6 weeks following transfer. Data are representative 5 mice per group. Results are shown as the means +/- s.e.m.

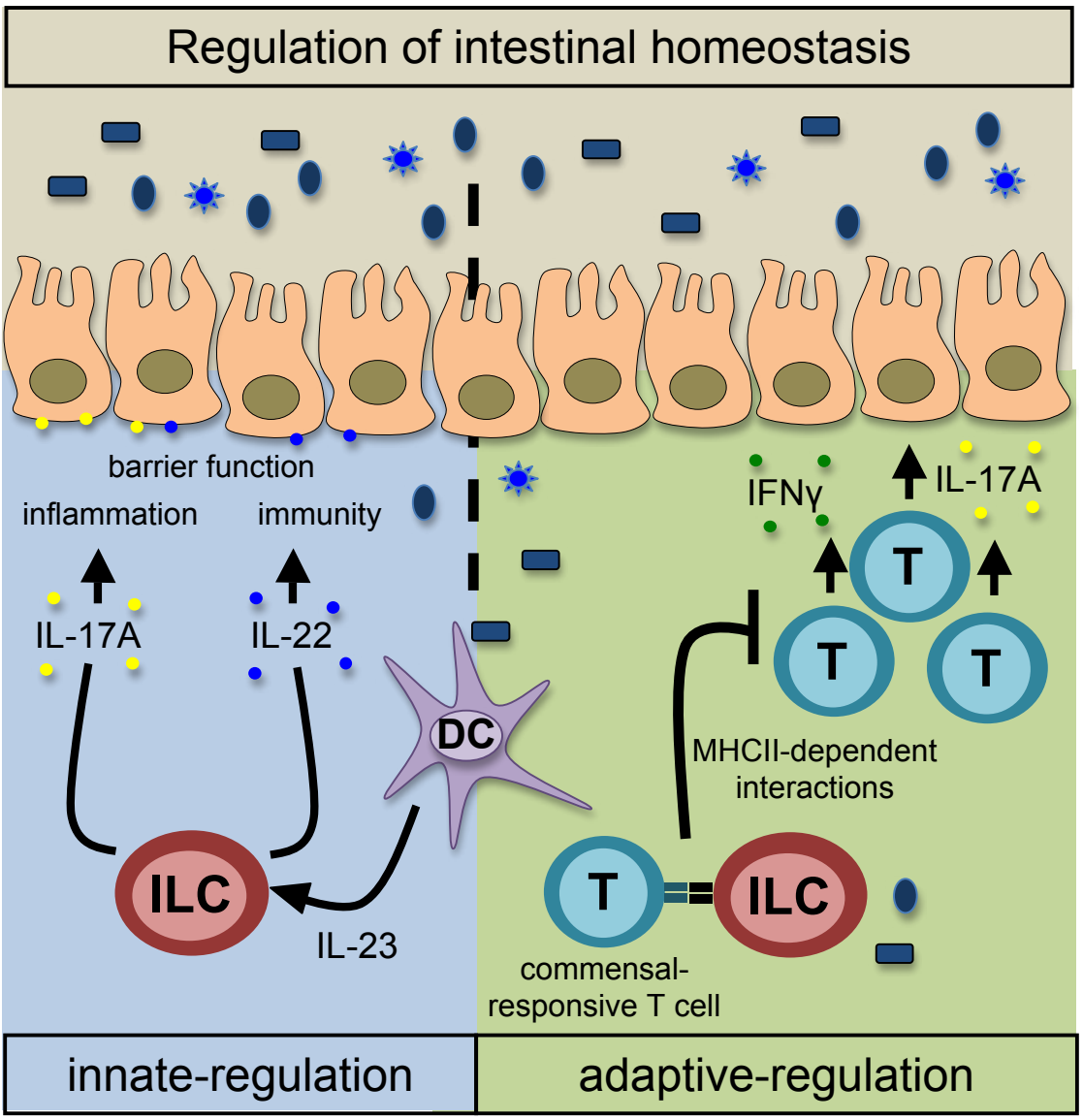

Figure S13. Innate lymphoid cells orchestrate intestinal homeostasis through regulation of innate and adaptive immune cell responses. Previous studies have identified that ILCs can influence intestinal homeostasis through innate cytokine-mediated regulation of intestinal epithelial cells. Production of IL-17A and IL-22 can act on intestinal epithelial cells to promote inflammation, innate immunity and regulate intestinal barrier function. In addition this report identifies that ILCs can modulate $CD4^+$ T cell responses to commensal bacteria through expression of MHCII. ILC-intrinsic MHCII limits the development of pathologic commensal bacteria-responsive $CD4^+$ T cells to orchestrate intestinal homeostasis.